Photon Sources
for Lithography and Metrology

Vivek Bakshi, *Editor*

SPIE PRESS
Bellingham, Washington USA

Downloaded From: https://www.spiedigitallibrary.org/ebooks/ on 11 Oct 2023
Terms of Use: https://www.spiedigitallibrary.org/terms-of-use

Library of Congress Cataloging-in-Publication Data

Names: Bakshi, Vivek, editor.
Title: Photon sources for lithography and metrology / Vivek Bakshi, editor.
Identifiers: LCCN 2022055893 | ISBN 9781510653719 (hardcover) | ISBN
9781510653726 (pdf)
Subjects: LCSH: Extreme ultraviolet lithography. | Laser plasmas. | Speckle
metrology. | Holography. | Ultraviolet radiation–Industrial
applications. | Lasers–Industrial applications.
Classification: LCC TK7872.M3 P473 2023 | DDC
621.3815/31–dc23/eng/20230113
LC record available at https://lccn.loc.gov/2021039247

Published by
SPIE
P.O. Box 10
Bellingham, Washington 98227-0010 USA
Phone: +1 360.676.3290
Fax: +1 360.647.1445
Email: books@spie.org
Web: https://spie.org

Copyright © 2023 Society of Photo-Optical Instrumentation Engineers (SPIE)

All rights reserved. No part of this publication may be reproduced or distributed in any form or by any means without written permission of the publisher.

The content of this book reflects the work and thought of the authors. Every effort has been made to publish reliable and accurate information herein, but the publisher is not responsible for the validity of the information or for any outcomes resulting from reliance thereon.

Images in lower portion of front cover are photographs of Energetiq Technology's Laser-Driven Light Source (LDLS™) bulb and Electrodeless Z-Pinch™ EUV plasma, used with permission.

Printed in the United States of America.
First printing 2023.
For updates to this book, visit https://spie.org and type "PM351" in the search field.

SPIE.

Downloaded From: https://www.spiedigitallibrary.org/ebooks/ on 11 Oct 2023
Terms of Use: https://www.spiedigitallibrary.org/terms-of-use

18 Tin Mitigation in EUV Sources **747**
Gianluca Panici and David N. Ruzic
18.1 Introduction 747
18.2 Multilayer Mirror Overview 749
18.3 Debris Mitigation 752
18.4 *In Situ* Tin Cleaning 758
18.4.1 Hydrogen radical etching 758
18.4.2 Hydrogen plasma etching 760
18.5 MLM Exposure to Hydrogen Plasma 767
18.6 Summary 768
References 770

PART V Lasers **775**

19 Compact Efficient CO_2 Amplifiers with Modular Design for High-Efficiency EUV Power Generation **777**
Koji Yasui, Jun-ichi Nishimae, Tatsuya Yamamoto, and Yuzuru Tadokoro
19.1 Background of EUV Applications for the United States 777
19.2 Concepts of CO_2 Lasers for EUV Generation 779
19.3 Scalability for >500-W EUV powers 784
19.3.1 500-W consideration based on experimental results 784
19.3.2 Further discussion on 1-kW EUV power 787
19.4 Modular Consideration for a Variety of EUV Applications 787
19.5 Summary 788
References 789

20 Excimer Lasers for Lithography **793**
Hakaru Mizoguchi, Osamu Wakabayashi, Toshihiro Oga, Hiroaki Nakarai, Hiroshi Komori, Kouji Kakizaki, and Junichi Fujimoto
20.1 Introduction 794
20.2 Excimer Laser–based Technology for Lithography Applications 795
20.2.1 Lithography exposure tool requirements on the light source 795
20.2.1.1 Average power and repetition rate 796
20.2.1.2 Pulse duration and stability 796
20.2.1.3 Maintenance interval and maintainability 797
20.2.1.4 Summary of requirements on the light source 797
20.2.2 Wavelength and bandwidth stabilization, and cavity design 797
20.2.3 Discharge chamber 798
20.2.4 Pulsed power module 799
20.2.5 Twin-chamber technology 800
20.3 Progress of DUV Lithography 803
20.3.1 Exposure tool 803
20.3.2 Practical excimer lasers for lithography 804
20.3.2.1 Overview 804

Downloaded From: https://www.spiedigitallibrary.org/ebooks/ on 11 Oct 2023
Terms of Use: https://www.spiedigitallibrary.org/terms-of-use

Chapter 18
Tin Mitigation in EUV Sources

Gianluca Panici and David N. Ruzic
University of Illinois Urbana-Champaign, Champaign, USA

18.1 Introduction
18.2 Multilayer Mirror Overview
18.3 Debris Mitigation
18.4 *In Situ* Tin Cleaning
    18.4.1 Hydrogen radical etching
    18.4.2 Hydrogen plasma etching
18.5 MLM Exposure to Hydrogen Plasma
18.6 Summary
References

18.1 Introduction

Every day, computers continue to infiltrate all facets of modern life, creating an enormous industry and encouraging innovation. The transistor is the initial invention that kickstarted this phenomenon. Gordon Moore of Intel, during the beginning of this technological movement, stated that every two years the number of transistors on an integrated chip must double to ensure that demand and innovation goals are met. The size of a transistor in 2001 was 0.25 μm.[1] The current industry standard in the 7-nm node is 14 nm for the half-pitch of the fins of the transistors. Technological advances have begun to run into physical constraints, slowing progress below Moore's prediction. Even the fact that the 7-nm node is 7 nm in "name only" when it is more than double that in feature size illustrates the problem.

To increase the number of transistors on a chip, the size of transistor features must decrease accordingly. The transistor manufacturing steps are traditionally called lithography, etching, and deposition. Lithography uses light to pattern a wafer. The patterns are then etched by either a chemical (wet etching) or plasma (dry etching) process. Finally, these patterns are filled by deposition. As both etching and deposition are fundamentally on the atomic

Downloaded From: https://www.spiedigitallibrary.org/ebooks/ on 11 Oct 2023
Terms of Use: https://www.spiedigitallibrary.org/terms-of-use

scale, the limiting step for Moore's law (to date) has been lithography. While photonic wavelengths near the atomic scale have been used in other applications, the flux of photons needed for high-volume manufacturing (HVM) in lithography severely limits the possible light sources for industry. Existing techniques such as multiple patterning and immersion lithography can reduce the pattern size but can only extend so far. This is the basis for the push for new, cost-effective lithography sources and the use of EUV light.

EUV lithography has been in development for decades but only recently has entered HVM fabrication plants (fabs). Yet, the throughput is still not at the level of current deep-UV (DUV) lithography. One of the challenges is collector contamination. To create the EUV light, molten tin (Sn) is injected into a vacuum chamber and struck with a powerful laser to create a plasma. The de-excitation of these Sn ions produces 13.5-nm photons. At this wavelength, nearly all materials absorb the photons, which means that new optics must be used. The only way to change the light path of these photons is by using a multilayer mirror (MLM), the largest of which is called the collector. These MLMs utilize Bragg reflection to partially reflect the photons. An overview of these optics is given in Section 18.2.

Contamination of the collector optic is one cause of EUV source downtime. The de-excited Sn collides with the walls and optics in the vessel, condensing into a film. This film absorbs EUV photons and must be cleaned off *ex situ*. Opening of the vacuum chamber and replacement of the collector optic lead to up to 24 hours of downtime in much of the installed base. Newer modular vessels reduce this by half or less. At a 50-kHz Sn droplet injection rate, the collector optic is typically swapped every 100 gigapulses or when reflectivity of the optic drops by 40% (Fig. 18.1).[2] Translating gigapulses into time and assuming all other parts are 100% functional, the collector is swapped every 24 days. The collector contamination alone attributes to ~4% downtime during the year, with other maintenance required for 24/7 operation. Worse yet, on the way to replacement, the reflectivity and therefore the throughput of wafers drops by half, so the productivity is severely constrained by the tin contamination. Contrasting this with DUV downtime of <1% in a year and full productivity during the remaining time, it is apparent that there is a long way to go for EUV lithography to overtake current technology completely in terms of throughput.

Current debris mitigation techniques include large amounts of gas to thermalize Sn ions and entrain them in the flow, allowing them to be pumped away. (Information about debris mitigation is covered in Section 18.3.) This method has been only partially successful, as the gas cannot completely stop particle momentum, and diffusion still leads to film buildup over time. *In situ* cleaning methods have been proposed, specifically, the use of hydrogen radicals that are already generated during the EUV pulse. Research concerning *in situ* cleaning with hydrogen radicals is presented in Section 18.4.1. Enhanced

Downloaded From: https://www.spiedigitallibrary.org/ebooks/ on 11 Oct 2023
Terms of Use: https://www.spiedigitallibrary.org/terms-of-use

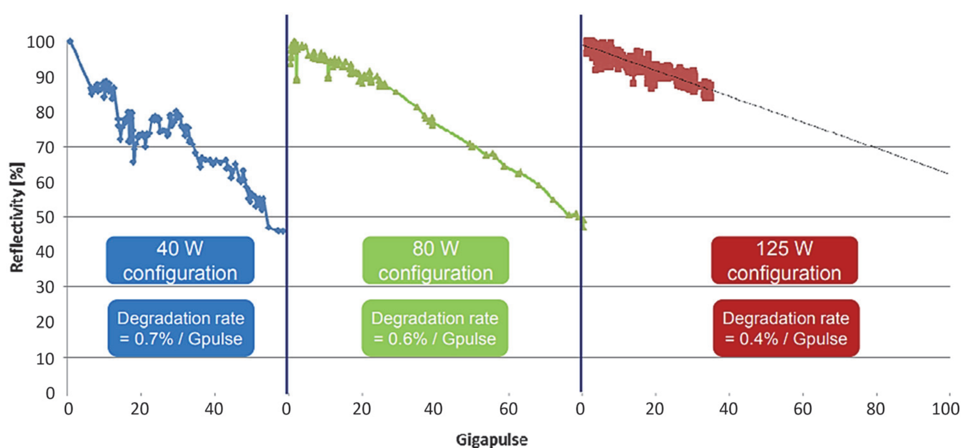

Figure 18.1 Degradation data for the collector optic in ASML EUV sources. This data was shown by ASML at the 2016 SPIE Advanced Lithography conference. Reflectivity is not a percentage of incident photons, but a percentage of reflectivity compared to initial values. The decrease in degradation rate as EUV power increases is attributed to the increase of hydrogen radicals as EUV power grows. (Reprinted from Ref. 2.)

cleaning efforts using plasmas can reach etch rates that radicals alone cannot attain. Research covering plasma-based efforts are discussed in Section 18.4.2.

Understanding these cleaning techniques in combination with debris mitigation is the first step to addressing the issue of collector contamination for the purpose of increasing tool lifetime for HVM integration.

18.2 Multilayer Mirror Overview

The EUV optics differ from their DUV counterparts as they are MLMs compared to the lens systems of the past. Upwards of 50 alternating layers of molybdenum (Mo) and silicon (Si) are used to build these mirrors atop of a substrate. Each pair of layers is called a bilayer. The difference in the index of refraction between the Mo and Si layers results in a small reflection of the photons of certain wavelengths, depending on the thickness of the layers. This is called Bragg reflection.[3,4] The bilayers are spaced at approximately half the wavelength of light to optimize reflection. While each bilayer reflection is small, the total sum of the stack can reach 70% at 13.5 nm.[5,6]

Molybdenum and silicon were chosen to maximize reflectivity of the bilayers while minimizing the absorption. To do this, the difference in the real part of the permittivities must be maximized while minimizing the imaginary part of the permittivity. This would maximize the reflection of each bilayer while minimizing the absorption of the photons. The relationships between the permittivities of each material in the bilayer are

Downloaded From: https://www.spiedigitallibrary.org/ebooks/ on 11 Oct 2023
Terms of Use: https://www.spiedigitallibrary.org/terms-of-use

$$f = \frac{\mathrm{Re}(\epsilon_1 - \epsilon_2)}{\mathrm{Im}(\epsilon_1 - \epsilon_2)}, \tag{18.1}$$

$$g = \frac{\mathrm{Im}(\epsilon_2)}{\mathrm{Im}(\epsilon_1 - \epsilon_2)}. \tag{18.2}$$

Material 1 is named the reflector, while material 2 is the spacer. Silicon was chosen as the spacer due to its low imaginary permittivity at 13.5 nm and thus low absorption. Mo is the reflector because the difference in real permittivity compared to that of Si is large. Reflectivity is maximized by maximizing f in Eq. (18.1) while minimizing g in Eq. (18.2). When discussing reflectivity, the peak value is quoted even though it is a spectrum that depends on the wavelength of incident photon. The theoretical reflectivity curve of the Mo/Si MLM can be calculated thanks to Lawrence Berkeley National Lab (LBNL).[7]

As shown in Fig. 18.2, even with perfectly deposited bilayers and normal incidence, peak reflectivity is 74%. MLM reflectivity can change during source operation due to the high temperature environment of the EUV source. Any thermal interdiffusion between the layers will result in a reflectivity loss due to changes to the material properties. Active cooling of the mirrors is a necessity in these vessels. In addition, the silicon is prone to oxidation, which will change its optical properties as well. A layer of ruthenium coats the top of the mirror due to its protection against oxidation.[8] The peak reflectivity of the mirrors aligns with the EUV spectra produced (see Fig. 18.3) so no additional gains can come from altering the mirrors.

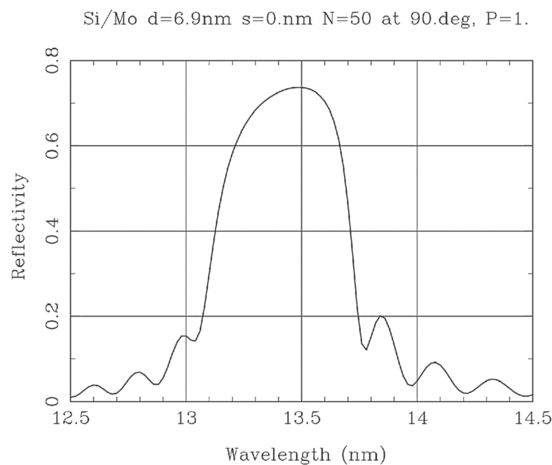

Figure 18.2 Reflectivity of a Mo/Si multilayer mirror with 50 bilayers as a function of incident photon wavelength. (Figure obtained using Center for X-ray Optics online calculator from Ref. 7.)

Downloaded From: https://www.spiedigitallibrary.org/ebooks/ on 11 Oct 2023
Terms of Use: https://www.spiedigitallibrary.org/terms-of-use

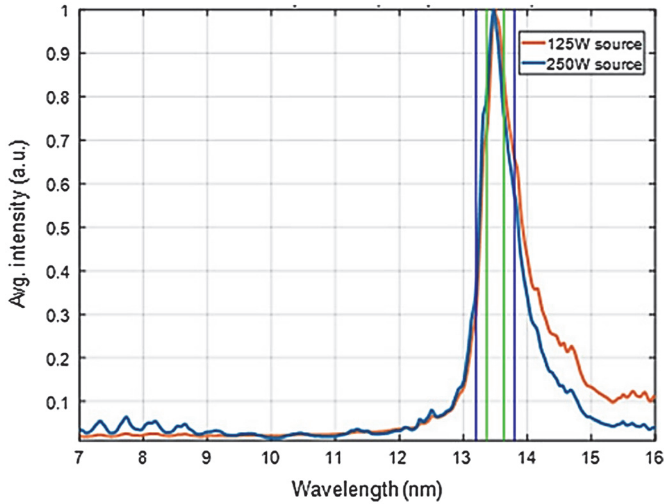

Figure 18.3 The EUV spectrum of the LPP at two different powers plotted as a function of wavelength (adapted from Ref. 9).

As stated earlier, the MLM partially reflects the incident photons. Modern mirrors reflect only up to 68% of the incident flux.[10] When considering reflectivity loss in the system, a drop of a few percentage points can contribute to a great loss in photons at the wafer surface due to the many mirrors that are needed. The EUV light path from source to wafer is shown in Fig. 18.4. If 100 W of EUV photons are created by the LPP and make it into the scanner, the wafer will see 1.0 W at best since there are 10 mirrors total.

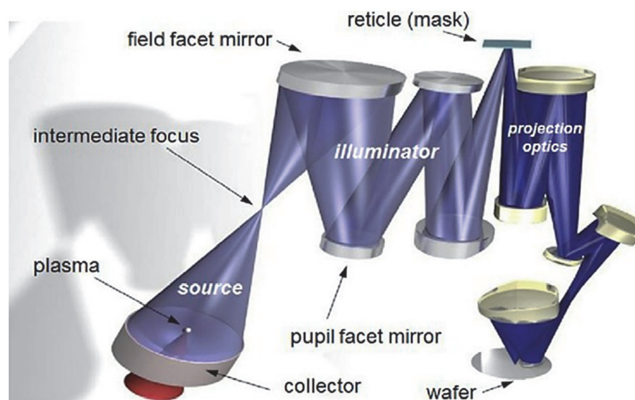

Figure 18.4 Illustration of the path the photons take from creation until wafer incidence. There are upwards of ten mirrors in the scanner alone. The light comes from the EUV source and bounces off each Bragg reflector. Each of these mirrors has, at most, 68% reflectivity, resulting in a power loss from source to wafer. Only 1% of the light that exits the source reaches the wafer. (Reprinted from Ref. 11.)

Downloaded From: https://www.spiedigitallibrary.org/ebooks/ on 11 Oct 2023
Terms of Use: https://www.spiedigitallibrary.org/terms-of-use

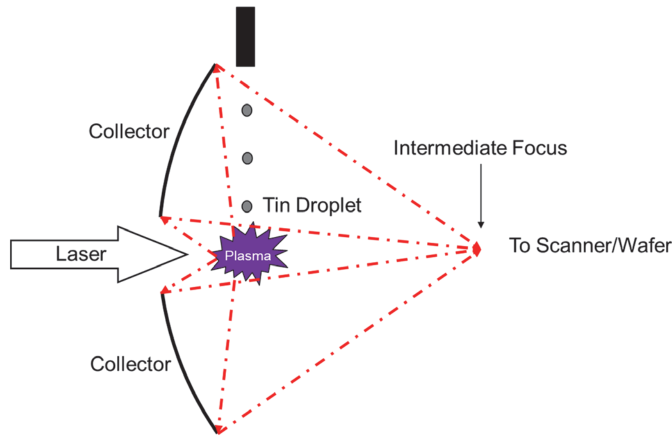

Figure 18.5 Schematic of the inside of the EUV source. The photons are created in a laser-produced plasma where they reflect off the collector and travel toward the scanner with the wafer. The collector optic sits in front of the LPP where it is subjected to tin debris deposition and the thermal load from the plasma.

The first optic in the optical chain is called the collector and is located within the EUV source environment, as shown in Fig. 18.5. This optic "collects" the photons as they are created and directs them towards the scanner. Due to its exposure to the LPP, the collector is the most prone to degradation from the debris that is generated during operation. Since a mirror is at best 70% reflective, a 10% loss in reflectivity at the collector would result in 13% loss of photons at the wafer surface. More likely, the collector efficiency is only 50%, so 10% loss of its reflectivity (i.e., dropping to 40%) means 20% fewer photons.

18.3 Debris Mitigation

Reflectivity degradation of the collector can be caused by sputter-induced roughness/erosion, energetic ion/neutral implantation, or Sn deposition. Sputtering of the collector is the most harmful degradation mechanism to reflectivity, especially if entire layers are sputtered away. One potential mitigation method for sputtering would be increasing the number of bilayers of the multilayer mirror. In principle, these excess bilayers can be sputtered away but would not affect the total reflectivity of the collector. In practice, however, the roughness and layer intermixing caused by sputtering renders this method to maintain reflectivity ineffective. The optimal number of bilayers for Mo/Si reflection of EUV is 40 to 50, as seen in Fig. 18.7. Above this number, the reflectivity becomes constant as a function of bilayers (Fig. 18.6), but the cost continues to increase.[12]

While EUV-producing plasmas have an optimal bulk temperature of approximately 30 eV,[13] the ion energy distribution contains a nontrivial

Downloaded From: https://www.spiedigitallibrary.org/ebooks/ on 11 Oct 2023
Terms of Use: https://www.spiedigitallibrary.org/terms-of-use

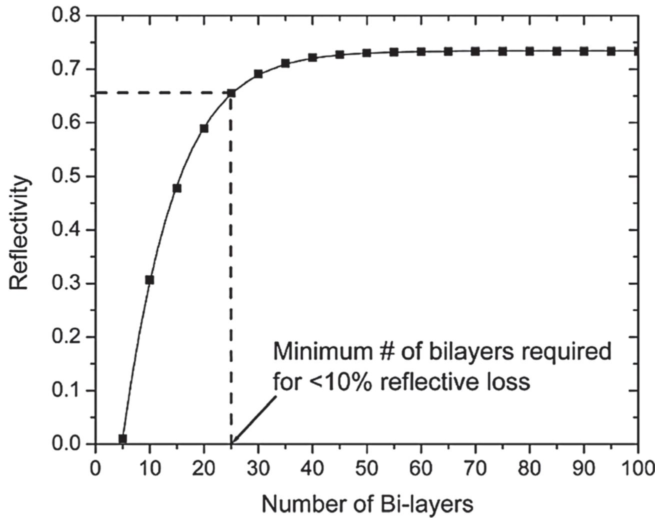

Figure 18.6 Calculation of the reflectivity of a Mo/Si multilayer mirror as a function of bilayer number. (Reprinted from Ref. 12 with permission of AIP Publishing.)

number of particles with keV energies. As the laser-produced plasma is created, higher-energy electrons will leave the initial volume first due to their low mass. A charge imbalance develops with excessive positive charge in the initial volume, leading to what is termed a *Coulombic explosion* with the ions repelling each other to high energies. In addition, these ions are pulled by the ambipolar electric field that develops in the wake of the fast electrons. These high-energy ions can reach multiple keV energies. Ions with these energies are the most problematic as they can easily sputter the collector or implant within the bilayers. The energy of the Sn ions can be lessened to some degree by the addition of hydrogen, since the hydrogen ions screen out some of the electric field accelerating the tin.[14] However, their energies remain well above the sputtering threshold.

One potential method of mitigating damage from charged particles is to magnetically deflect them from the collector. Magnetic mitigation takes advantage of the high energies that make this energetic debris troublesome. The faster the velocity of the incoming particle, the larger the deflection force by the magnetic field. This is illustrated in Eqs. (18.3) and (18.4):

$$\mathbf{F} = q\mathbf{v} \times \mathbf{B}, \tag{18.3}$$

$$v = \sqrt{\frac{2E}{m}}, \tag{18.4}$$

where $\mathbf{F}$ is the force, q is the charge on the particle of mass m moving with velocity $\mathbf{v}$ in a magnetic field $\mathbf{B}$. The kinetic energy of the particle is E.

Downloaded From: https://www.spiedigitallibrary.org/ebooks/ on 11 Oct 2023
Terms of Use: https://www.spiedigitallibrary.org/terms-of-use

Academic and industrial applications of this mitigation technique have been studied and implemented. One such work used a 0.5-T (tesla) magnetic field to deflect ions from a laser-produced plasma generated using a solid tin target.[15] The average ion energy was measured to be 1.2 keV. Ion flux was measured using a Faraday cup, which records charge as a function of time. This Faraday cup was positioned 15 cm from the source at an angle of 66 deg. Ion flux at the Faraday cup was reduced by nearly an order of magnitude in the presence of the magnetic field (Fig. 18.7).

Endo and colleagues from the Extreme Ultraviolet Lithography System Development Association in Japan have tested magnetic mitigation using a 1-T field in a Sn-fueled LPP akin to industrial EUV systems.[16] Introduction of the magnetic-field-reduced the ion signal on the Faraday cup to noise levels (Fig. 18.8).

One commercial EUV source manufacturer is pursuing magnetic mitigation: Gigaphoton.[17] A reproduction of their debris mitigation scheme is shown in Fig. 18.9. Magnets are used to trap low-energy ions and to attempt to deflect high-energy ions. Unfortunately, while magnets may help mitigate the charged debris, there are still high-energy neutrals that are generated from ion-neutral charge exchange and recombination.[18] Revisiting Endo's work,[16] the ion debris is estimated to be much less than the total debris (∼1%). This is reconfirmed with quartz-crystal microbalance (QCM) measurements that

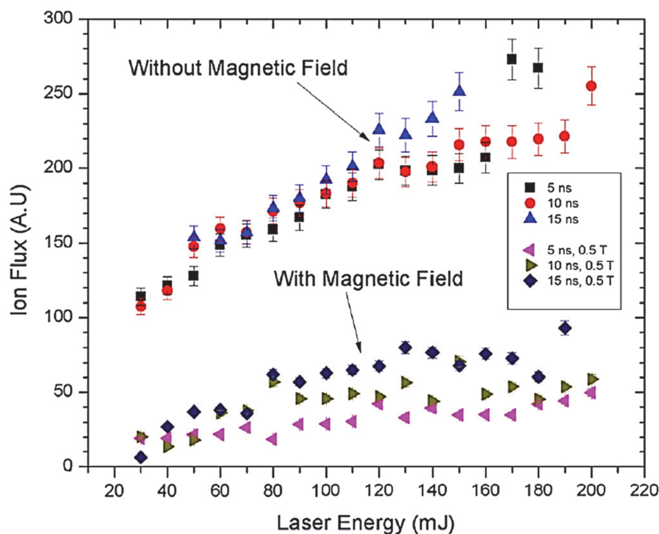

Figure 18.7 Ion flux from a solid target LPP measured using a Faraday cup 15 cm from the source at an angle of 66 deg. Pulse energy and duration were varied for the ablation of the solid Sn target. The measured ion flux is reduced by nearly an order of magnitude in the presence of the magnetic field, regardless of pulse energy or duration. (Reprinted from Ref. 15 with permission of AIP Publishing.)

Downloaded From: https://www.spiedigitallibrary.org/ebooks/ on 11 Oct 2023
Terms of Use: https://www.spiedigitallibrary.org/terms-of-use

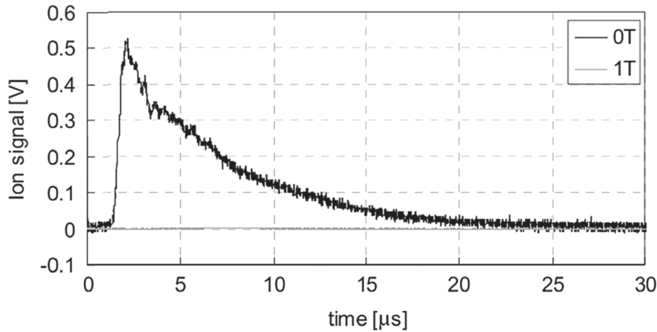

Figure 18.8 A Sn-fueled LPP similar to industrial EUV sources was used to test the viability of magnetic mitigation. In the presence of the 1-T magnetic field, the ion signal on the Faraday cup was reduced to near zero, comparable to noise. (Reprinted from Ref. 16.)

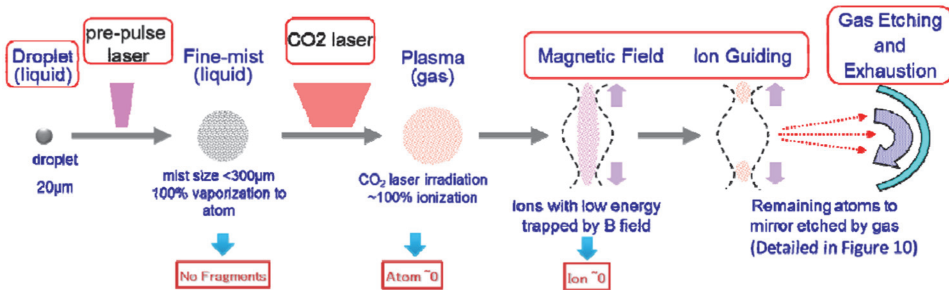

Figure 18.9 Schematic of magnetic mitigation scheme in development for Gigaphoton EUV sources. (Reprinted from Ref. 17.)

Endo performed showing nearly no reduction in Sn deposition rate with magnetic field (Fig. 18.10).

As most debris from the LPP is neutral Sn, magnetic deflection will not be sufficient to alleviate damage concerns. A separate technique must be utilized that will decrease debris energy and deflect these particles away from the collector regardless of charge state. The chosen mitigation technique in modern systems is to use a *buffer gas* to slow the debris and direct it away from the collector. While this is the preferred method of industry, few studies have looked at the transport of both energetic ions and neutrals to the collector in the presence of a buffer gas. However, Sporre et al. modeled and measured the impact of buffer gas on both ion and neutral flux at the intermediate focus (IF) from a discharge-produced plasma as a function of pressure using a spherical energy sector analyzer (Fig. 18.11).[19] The IF is the point at which the photons converge toward the scanner, as shown in Fig. 18.5. Energetic debris can cause damage to the optics in the EUV scanner as well as to the collector.

Downloaded From: https://www.spiedigitallibrary.org/ebooks/ on 11 Oct 2023
Terms of Use: https://www.spiedigitallibrary.org/terms-of-use

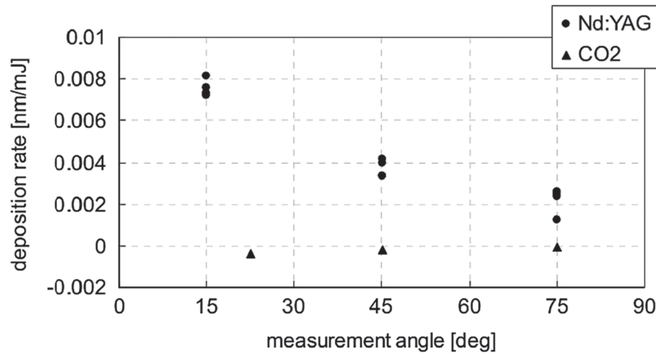

Figure 18.10 QCM measurements of the deposition during operation of a Sn-fueled LPP with and without magnetic mitigation. The deposition rate is not influenced greatly by the 1-T field, suggesting that most debris is uncharged. (Reprinted from Ref. 16.)

For this work, the chamber had an operating pressure of 0.3 mTorr with no buffer gas. An XTREME Technologies XTS 13-35 z-pinch was used to create the 30-eV EUV plasma. Nitrogen gas was used as the pinch fuel, while argon was the buffer gas. Microchannel plates, along with an electrostatic ion deflector, were used to measure energetic neutrals that reached the IF. At 0.3 mTorr, there is no buffer gas and most of the pinch is lost to the walls. With low background gas density, scattering events are minimal and only ~7.75% of the total initial energy is deposited in the buffer gas.[18] This leads to ~0.1% of the energy reaching the IF. Thus, the data points at 0.3 mTorr in Fig. 18.11

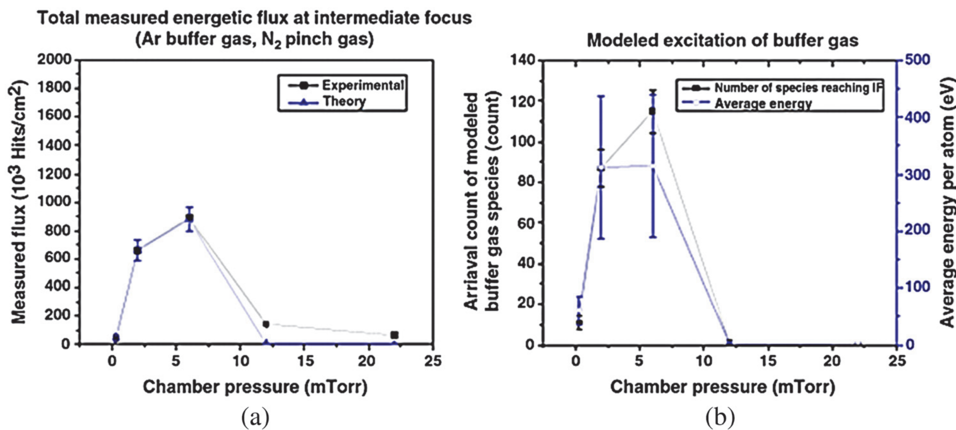

Figure 18.11 (a) The theoretical and experimental debris flux at the IF plotted as a function of chamber pressure. With no buffer gas, the operating pressure is 0.3 mTorr. As buffer gas is introduced, the energy transfer to the gas increases and the detected flux increases. There is a significant reduction in flux after 10 mTorr due to increased collisions with the background gas that now scatter energized neutrals. (b) The average energy and number of atoms at the IF. Both the number and the average energy of particles decrease after 10 mTorr due to the higher collisionality of the plasma. (Reprinted from Ref. 19.)

Downloaded From: https://www.spiedigitallibrary.org/ebooks/ on 11 Oct 2023
Terms of Use: https://www.spiedigitallibrary.org/terms-of-use

correspond to nearly no flux to the IF. Instead, the energy in the EUV source would be deposited at the walls or collector. Once buffer gas is introduced, the energy transfer to the background gas can energize the argon and create an apparent rise in the IF flux. Only after the pressure increases above 10 mTorr do the energetic debris flux scatter and decrease from collisions with the buffer gas. At this point the average energy of energetic species also decreases due to the collisions with background gas.

While this data may seem to suggest that pressure is the dominant mechanism for ion energy/flux reduction, in this case the higher collisionality at higher pressures causes more scattering and energy transfer to the buffer gas. In turn, this reduces the energy and flux of debris at the IF. This also means that the energy of the debris within the EUV source drops as well due to the increased pressure. It is important to note that a static background gas will not have the intended deflection or scattering. As most of the collisions the ions will undergo are forward scattering, they would at best charge exchange with the background gas. Returning to the collector, these energetic ions-turned-neutral particles may still have a trajectory that would impact the collector surface. A large flow rate is needed to change the direction of these fast particles, entrain any that have slowed down, and carry them to the vacuum pump inlet. For the flowing gas to have this effect, its resident time must be on the same order of magnitude as the diffusion time constant of the ion and neutral species. The affected flux will then be modified:

$$\Gamma = \Gamma_0 \exp\left(\frac{\tau_D}{\tau_{gas}}\right), \tag{18.5}$$

where the initial flux is given by Γ_0, and the final flux by Γ. The important factor is the exponential ratio of the diffusion time of the species τ_D to the resident time of the gas τ_{gas}. According to ASML, the buffer gas that is chosen for their commercial EUV sources is hydrogen due to its high heat capacity, thermal conductivity, and EUV transparency.[20] Using a variety of flow rates and pressure recipes, ASML has been able to significantly slow down the collector degradation (see Fig. 18.12 with 0.04% degradation per gigapulse as compared to Fig. 18.1 at 0.4%).[21] An increase in pressure is used to eliminate contributions from particle diffusion. At this point, the debris profile is affected by the hydrogen flow profile. The hydrogen flow not only slows down the Sn vapor but entrains it, redirecting the debris towards the walls and exhaust.

As the collector lifetime has been defined by industry as the time until collector reflectivity drops to 50%, current efforts have only just begun to reach the target of 1000 gigapulses without collector swap for 250-W sources. As HVM requirements dictate higher EUV power of at least 500 W, this degradation rate is still inadequate. Assuming 50 kHz and 0.08%/gigapulse

Downloaded From: https://www.spiedigitallibrary.org/ebooks/ on 11 Oct 2023
Terms of Use: https://www.spiedigitallibrary.org/terms-of-use

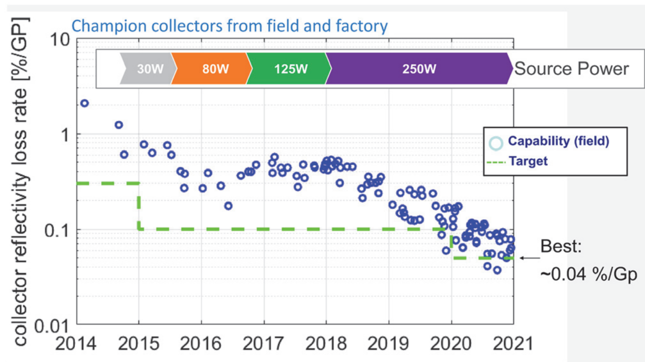

Figure 18.12 Using H_2 as a buffer gas, ASML has succeeded in slowing down the collector degradation in comparison to Fig. 18.1. (Reprinted from Ref. 21.)

degradation for a 500-W source, this amounts to a 625-gigapulse lifetime or about 144 days. Comparing this to the aforementioned 24-day lifetime that is typical of much of the installed base, it's clear that additional efforts are needed to reduce collector contamination.

This contamination can be separated into two categories: "fast" and "slow." The high-energy debris that incorporates fast contamination has been shown to be successfully mitigated using a buffer gas. The slow contamination is in the form of Sn that is ejected from nearby walls or other surfaces in the chamber. In addition, agglomeration of the tin (tin bunching up into balls) from the EUV plasma can occur. These are particles from other surfaces and large; agglomerated particles cannot be stopped by the small hydrogen gas molecules and are the major contributors to collector reflectivity degradation. To extend the collector lifetime, *in situ* collector cleaning must be developed to supplement mitigation techniques. The next section is dedicated to the potential avenues of tin cleaning techniques using hydrogen radicals and plasma.

18.4 *In Situ* Tin Cleaning

18.4.1 Hydrogen radical etching

Debris management involves removal of the tin from the source without impact to the EUVL source lifetime. This is an inherently *in situ* method and involves cleaning the tin from the walls with a chemically reactive gas. Fortunately, hydrogen is chemically reactive with tin. If radicals are formed, four hydrogen radicals will react with one tin atom, forming a gaseous stannane that can be pumped away from the vessel:

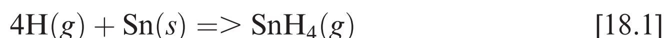

$$4H(g) + Sn(s) => SnH_4(g) \quad [18.1]$$

Downloaded From: https://www.spiedigitallibrary.org/ebooks/ on 11 Oct 2023
Terms of Use: https://www.spiedigitallibrary.org/terms-of-use

Recalling Fig. 18.1, the decrease in degradation rate correlates with an increase in EUV power. Why? The increase in EUV power also results in an increase in out-of-band radiation (photons that are outside of the range that can be reflected by the MLM). These auxiliary photons have a non-negligible absorption cross-section with the background hydrogen (Fig. 18.13). As these photons interact with the hydrogen gas, they are absorbed. This generates a H^* population that can then react with the deposited Sn atoms. In addition, the photons that are not stopped in the gas will reach the walls and cause electron emission due to the photoelectric effect. These photoelectrons can dissociate hydrogen near the walls. Finally, the expansion of the plasma from primary focus will also ionize and dissociate hydrogen gas. The creation of all of these radicals has been referred to as the 'self-cleaning' aspect of the EUV source. Unfortunately, it cannot overcome the deposited Sn flux and must be supplemented somehow. The current method of cleaning is *ex situ*, which increases tool downtime. There have been proposals to introduce external hydrogen radical sources that generate a large density of H^* and blow them into the vessel. One example of such a method was used by van Herpen et al. to clean a 10-nm Sn film from an EUV optic.[23]

One drawback of this technique is the cleaning rate. An initial rate of 28 nm/min was seen, but as the 10-nm film became thinner, this dropped to 0.3 nm/min. The thought was that redeposition of the etch product (SnH_4) after the initial etch resulted in a severe drop-off of the cleaning rate.[23]

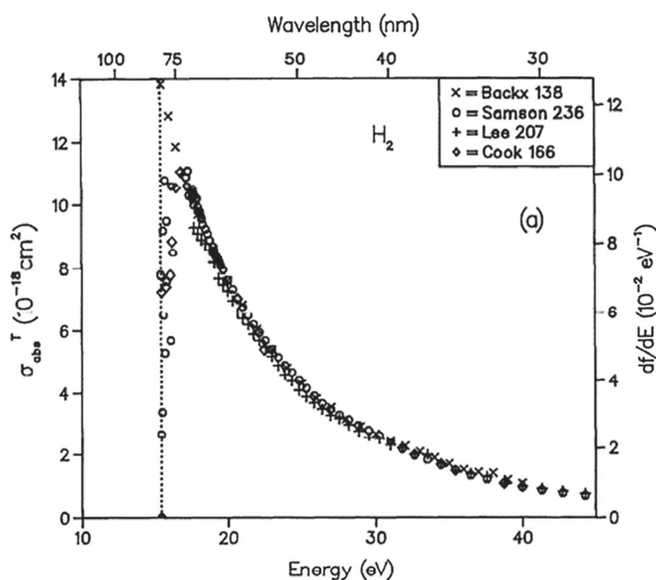

Figure 18.13 The total photo-absorption cross section of photons from 30 to 100 nm by molecular hydrogen. Partial contributions include the photoionization and photon-induced dissociation reactions. (Reprinted from Ref. 22 with permission of AIP Publishing.)

Downloaded From: https://www.spiedigitallibrary.org/ebooks/ on 11 Oct 2023
Terms of Use: https://www.spiedigitallibrary.org/terms-of-use

A practical drawback is the delivery system for these hydrogen radicals. While van Herpen et al.[23] used a tungsten filament in vacuum near the sample to be etched, this is not possible within the EUV source. Instead, an external generator would need to be implemented with radicals blown in through a quartz tube; however, flow would need to be optimized to direct radicals toward the collector. This would be counter-productive since the buffer gas must flow away from the collector to block debris. Recombination of the radicals on surfaces, such as the quartz tube that directs them into the vessel, would decrease radical flux before it reached the collector. In addition, cleaning rates must be high enough to overcome redeposition of stannane that has been shown to thermally decompose readily above 100 °C, especially if it hits a tin-covered surface.[24]

A different technique is needed to generate hydrogen radicals at the collector surface to be etched. The etch rate must also be maximized to overcome redeposition in the source environment. A plasma-based *in situ* method has been proposed to accomplish both tasks: plasma generation can generate radicals near the surface, and the combination of radicals and ions has been proven to etch faster than radicals or ions alone.

18.4.2 Hydrogen plasma etching

Plasma etching is commonly used to remove material from silicon wafers during the transistor manufacturing process. Not only does plasma-based removal create reactive species near the surface to be modified, but it also creates ions that impart energy to the surface. In the now-famous experiment by Coburn and Winters, silicon was etched in fluorine chemistry using the common precursor XeF_2. An argon ion beam was then turned on for a length of time. Finally, the XeF_2 gas was stopped, and the ion beam's silicon etch rate was obtained. The results are shown in Fig. 18.14, which is from their ground-breaking paper.[25] While this is not a plasma-based etch itself, it is meant to simulate the conditions to be found during plasma processes. In other words, both ions and radicals are present in these experiments as well as when creating a plasma. The conclusion that Coburn and Winters came to was that etch product volatility was increased during the period of sample exposure to radicals and ions. In addition, the role of ion bombardment was hypothesized to be an increased energy flux to the surface, assisting in formation of these volatile etch products.

Research behind tin removal processes by plasma has been performed in the past for the purpose of cleaning the collector. Before the EUV fuel and background gas were chosen, a mixture of argon (Ar) and chlorine (Cl) was proposed by Shin et al. for tin etching purposes.[26] Chlorine will chemisorb to tin, eventually forming a volatile $SnCl_4$. In addition, Shin et al. note that argon ion bombardment helps to form dangling bonds on the surface, creating sites that are actively filled by physisorbed or chemisorbed chlorine atoms.

Downloaded From: https://www.spiedigitallibrary.org/ebooks/ on 11 Oct 2023
Terms of Use: https://www.spiedigitallibrary.org/terms-of-use

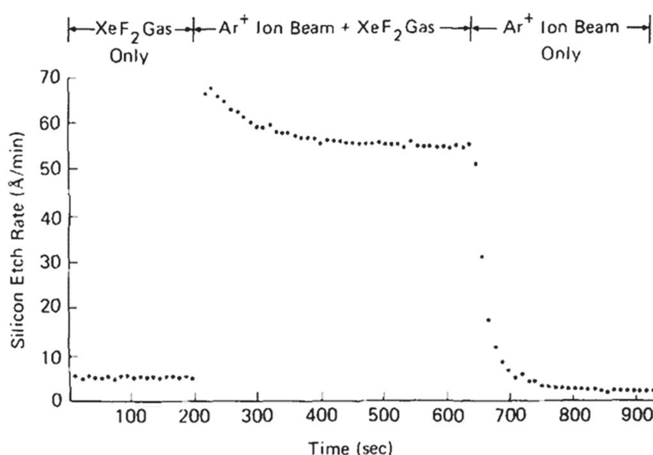

Figure 18.14 Coburn and Winters observed etch enhancement of silicon when both radicals and ions were incident on the surface. This is attributed to the increased volatility of the etch product. (Reprinted from Ref. 25 with permission of AIP Publishing.)

This mirrors the Coburn–Winters hypothesis of the enhanced etch mechanism in the fluorine–silicon system. In addition to plasma–material interactions, the chemisorbed, partially formed etch products (SnCl, $SnCl_2$) will react on the surface due to the Langmuir–Hinshelwood mechanism[26,27] and form volatile $SnCl_4$. This is also believed to be true in the tin–hydrogen system, but there has been no work to prove the validity of this hypothesis.

The plasma used in the work of Shin et al.[26] was an inductively coupled plasma (ICP) utilizing radiofrequency (RF) power (with frequency 13.56 MHz) running through a coil and a RF bias on the sample to increase ion energy at the surface. Samples were exposed to a combination of 10 standard cubic centimeters per minute (sccm) of Ar and 20 sccm of Cl_2. Etch rates of tin and other materials commonly found in EUV sources are shown in Fig. 18.15. In 2008, the time of the paper,[26] ruthenium (Ru) and silicon (Si) were thought to be common capping layers to protect the collector surface. Silicon dioxide (SiO_2) was included to measure etching of the native oxide of the silicon. An impressive micron per minute etch rate was achieved for tin, overcoming any potential redeposition concerns. Unfortunately, silicon was also etched at 15 nm/min. Any exposed bilayer of the multilayer mirror would be etched away, making this an unviable etch chemistry. In addition, chlorine is a difficult processing gas to work with, and costly upgrades would need to be made.

These data do show an interesting trend in RF bias. As bias voltage increased, presumably so did the ion energy and subsequent flux to the sample surface. This, in turn, seemed to enhance the tin etch rate, with a significant jump when changing the RF bias from −70 to −85 V. While this cannot be directly correlated to ion energy (no measurements of this were performed), it

Downloaded From: https://www.spiedigitallibrary.org/ebooks/ on 11 Oct 2023
Terms of Use: https://www.spiedigitallibrary.org/terms-of-use

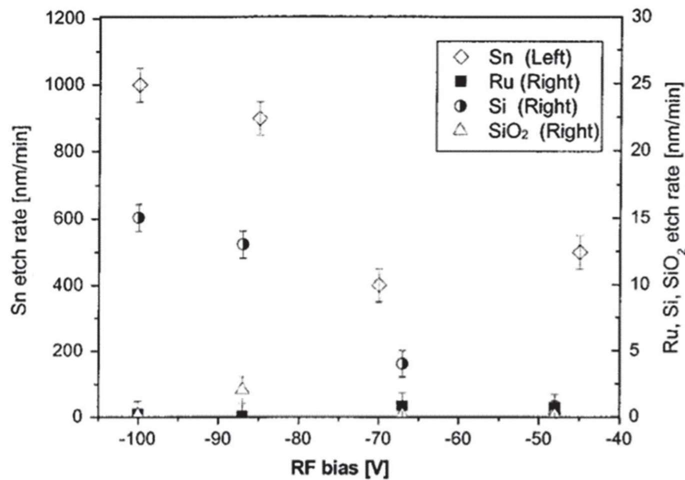

Figure 18.15 H* etch rate results for materials commonly found in EUV source devices. As RF bias increases, the ion energy flux to the surface increases as well. This enhances the etch rate by the mechanisms hypothesized by Coburn and Winters. (Reprinted from Ref. 26 with permission of AIP Publishing.)

does lend validation to the hypothesis that a plasma-based approach with substantial ion flux will be able to overcome tin redeposition in an EUV source. Sporre et al. continued this work by using hydrogen chemistry to etch tin.[28] A helicon source was used to generate remote plasma that would, through diffusion, travel to the sample surface and etch tin away. Etch rates in the tens of nm/min range were achieved, but the results were not reproducible. The low ion energy and flux would most likely not be able to etch larger samples than the 1-cm^2 Sn-coated Si used in the work. For collector-scale etching, the remote helicon source was deemed inadequate. Transport of the plasma from source to sample reduces ion and radical flux through recombination in the gas and at surfaces.

An *in situ* solution that creates plasma at the surface to be etched is required for optimal etch rates in hydrogen chemistry. One such solution proposed by Elg et al. uses a capacitively coupled plasma (CCP).[29] The collector itself was proposed as the RF electrode to create this plasma; not only did this result in ions and radicals near the surface, but the RF self-bias (that is inherent to CCP systems) increased the ion energy and flux. In turn, it was theorized that the etch rates of Sn by hydrogen would be enhanced. As evident in Fig. 18.16, this was *not* the case. Etches were performed at pressures below 1 Torr, resulting in lower-than-ideal radical and plasma densities ($\sim 10^{12}$ cm^{-3} and $\sim 10^{10}$ cm^{-3}, respectively).[30] This would, however, increase the mean free path of ions and result in a large ion energy impact at the surface. Indeed, Elg[29] observed a correlation between etch rate and ion energy flux (ion energy at surface H* ion flux). This seems to be a measurement of the

Downloaded From: https://www.spiedigitallibrary.org/ebooks/ on 11 Oct 2023
Terms of Use: https://www.spiedigitallibrary.org/terms-of-use

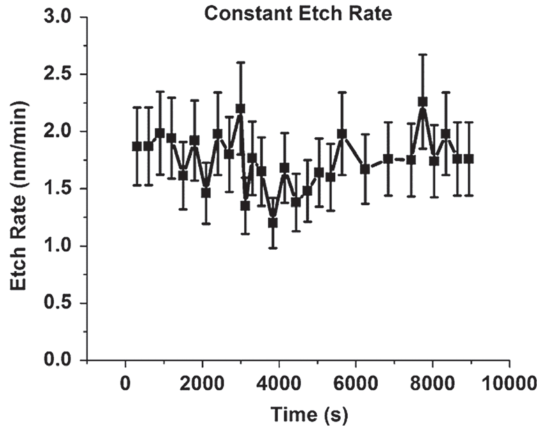

Figure 18.16 A series of etches performed using the collector as a RF electrode, driving a capacitively coupled plasma. Etching was performed in 5-min segments to reduce the probability of oxidation by thermal load due to plasma. (Reprinted from Ref. 29 with permission of Springer Nature.)

rate at which ions impart energy to the surface, increasing dangling bonds on the surface. Etch product volatility presumably increased as well, validating the Coburn–Winters theory. Figure 18.17 shows this correlation for low pressures.

Another figure of merit that has been studied for the tin–hydrogen etch system is the number of hydrogen radicals required to etch a single tin atom. An initial study was performed by Ugur et al. using only hydrogen radicals to etch a tin-coated QCM.[31] The source of hydrogen was a tungsten filament that created a flux of $3.2\times10^{17}\,\mathrm{H^{*}cm^{-2}s^{-1}}$. Measuring the amount of etched tin, Ugur et al.[31] converted this to tin atoms that were removed from the

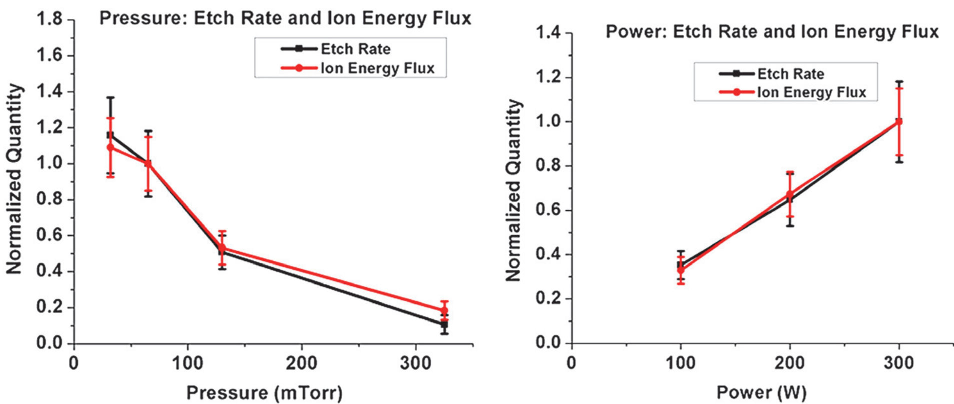

Figure 18.17 Tin etch rates observed to scale with ion energy flux to the sample surface. This phenomenon is independent of (left) pressure and (right) plasma input power. (Reprinted from Ref. 29 with permission of Springer Nature.)

Downloaded From: https://www.spiedigitallibrary.org/ebooks/ on 11 Oct 2023
Terms of Use: https://www.spiedigitallibrary.org/terms-of-use

surface and were able to calculate that 90,000 hydrogen radicals were required to etch a single tin atom. In a work of Elg et al.,[29] the CCP generated a flux that was quite similar (4.2×10^{17} $H^{*}cm^{-2}s^{-1}$). They also performed this figure of merit calculation and found that, in the presence of hydrogen ion energy flux of 4.6 kW/m^2, 2500 H^{*} were required per Sn atom etched. This further validates the Coburn–Winters hypothesis that chemical etching is enhanced by ion bombardment. The ion flux creates more dangling bonds for the radicals to attach to compared to etching with radicals alone. While Coburn and Winters showed this for fluorine etching silicon, Elg[29] proved its validity for the tin–hydrogen system.

Finally, the hydrogen plasma must be able to restore reflectivity to the collector surface. MLM samples were coated and exposed to the hydrogen plasma (Fig. 18.18), showing reflectivity restoration.[32] The control samples were untouched, the bare samples had no tin deposited on them, the etched samples were only exposed to hydrogen plasma, the deposited samples only had tin deposited, and the deposited & etched samples were deposited with tin and then etched. The samples were placed on a dummy aluminum collector that was coated with tin as well. The reflectivity was restored by the hydrogen plasma, validating this technique for debris management.

Extension of the collector-driven plasma to industrial pressures does not seem viable given the decreasing slope as pressure increases [see Fig. 18.17 (left)]. Increasing power can increase density, but introducing a RF bias to the collector brings other concerns. The collector itself cannot be used as the electrode due to the RF self-bias. The bias accelerates hydrogen ions to

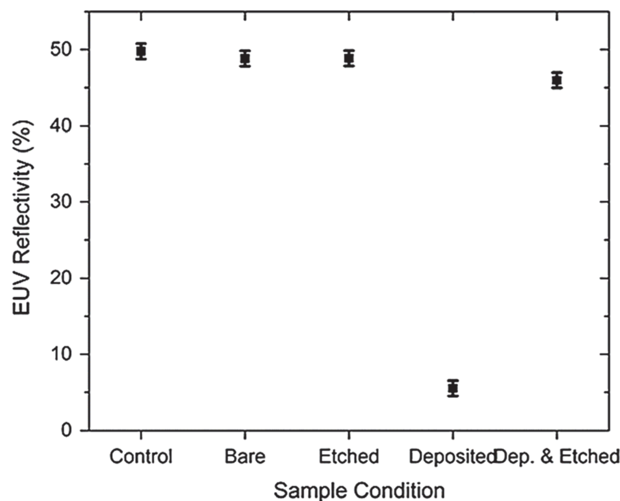

Figure 18.18 EUV reflectivity measurements of various MLM samples. Etched samples were exposed to hydrogen plasma, while deposited samples were coated with a Sn film. (Reprinted from Ref. 32 with permission of AIP Publishing.)

Downloaded From: https://www.spiedigitallibrary.org/ebooks/ on 11 Oct 2023
Terms of Use: https://www.spiedigitallibrary.org/terms-of-use

energies that can sputter or implant. Recalling that there are also Sn ions in the system that would be accelerated when the purpose of the buffer gas flow is to decelerate and stop them, an alternative plasma-based method is needed. In addition, etch rates higher than the demonstrated 2 nm/min would be desired to overcome redeposition in today's systems. Ideally, a plasma with high density, low electron temperature, and no self-bias would be created at the collector surface using specialized hardware that is added to the source.

A surface-wave plasma (SWP) can provide high plasma density with low electron temperature and the ability to be generated at industrial pressures without utilizing the collector as an electrode. Work has been done at the University of Illinois exploring various types of SWP antennas that can partially coat the collector with plasma and keep reflectivity from degrading.[33–35] One particular antenna was embedded within the collector cone that sits within the center hole, and plasma was extended from this cone out onto the collector. The setup was tested on an intentionally Sn-contaminated collector at ASML San Diego. A photograph of the experiment is shown in Fig. 18.19. The cone source was placed onto this collector with macroscopic surface roughness, indicating a film on the millimeter scale. Tin-coated silicon samples were then placed onto this collector surface. This constituted a worst-case scenario for being able to remove Sn contamination; where the full plasma volume could not be generated, there was poor thermal contact between samples and collector, and the vast amount of tin could redeposit onto the potentially hot samples.

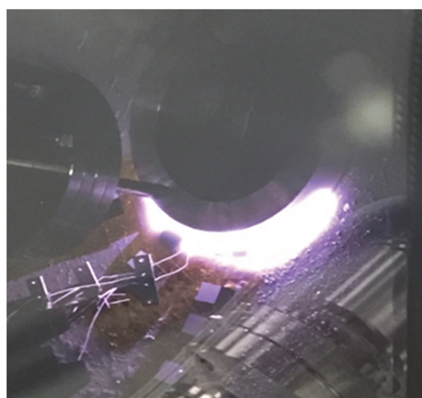

Figure 18.19 Hydrogen surface-wave plasma extending from cone source onto an intentionally Sn-coated collector with Sn-coated silicon samples on top to measure the etch rate. With an input power of 100 W at 600 MHz, there was not enough plasma generated to cover the entire collector. (Reprinted from Ref. 35.)

Downloaded From: https://www.spiedigitallibrary.org/ebooks/ on 11 Oct 2023
Terms of Use: https://www.spiedigitallibrary.org/terms-of-use

A radial scan of etch rates and radical densities was taken for two separate flow cases: from inside the cone [+ž direction, which is perpendicular to the collector if the center of the cone source (see Fig. 18.19) is the origin] and from the perimeter of the collector (–ř direction, across the collector). The cone flow was thought to not affect the plasma as the cone source is shielding the SWP from flow. The perimeter flow would act counter to what is desired, blowing the volatile tin hydride back towards the plasma, and increasing redeposition due to thermal decomposition. The results from these two tests are shown in Fig. 18.20.

As expected, when comparing the perimeter flow and cone flow cases, the former had a lower etch rate overall. Even with the contrary flow, the perimeter case was able to etch 1 nm/min all the way to 9 cm from the antenna. The cone case had a higher etch rate at 9 cm (1.5 nm/min) without the extra tin hydride flux from the perimeter flow. Another interesting result was that the radical density was higher for the perimeter case due to the radicals being trapped by the –ř flow. Even so, the etch rate was lower. These data are another example of the importance of the ion energy flux compared to hydrogen radicals alone. Ongoing work is being performed at the University of Illinois to estimate the required input power for a SWP to etch the entire collector.

In this section we have seen that a H plasma is very good at cleaning the collector. Before it can be implemented intentionally, the effect that a hydrogen plasma may have on the MLM must be investigated. Therefore, much research and effort has been invested into mitigating debris damage. However, the industrial EUV source already has a hydrogen plasma present from photon–gas interactions with the buffer gas (refer to beginning of

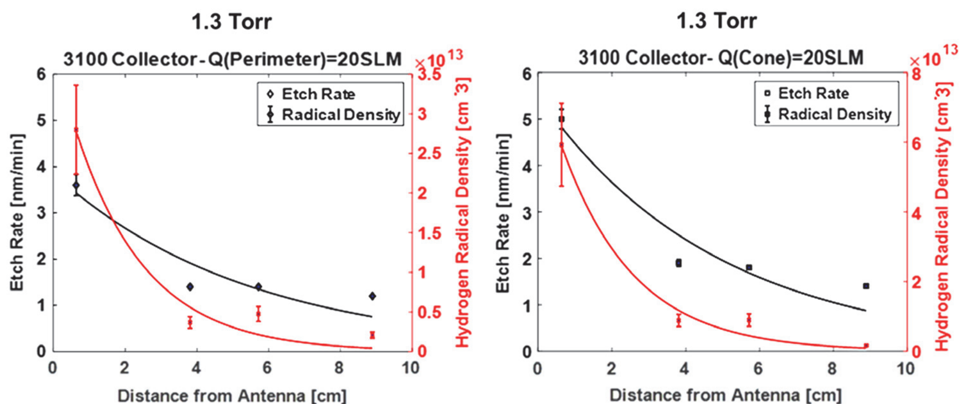

Figure 18.20 (left) Perimeter flow experiment and (right) cone flow experiment. Even with a dirty collector underneath the samples and contrary flow, the perimeter flow case shows 1 nm/min etch rate all the way to 9 cm from the antenna. (Reprinted from Ref. 35.)

Downloaded From: https://www.spiedigitallibrary.org/ebooks/ on 11 Oct 2023
Terms of Use: https://www.spiedigitallibrary.org/terms-of-use

Section 18.4.1), so adding more plasma may not be harmful. The next section investigates potential effects from the plasma.

18.5 MLM Exposure to Hydrogen Plasma

Even in the absence of *in situ* plasma cleaning techniques, the EUV-induced background plasma exists. In the EUV scanner, without the presence of buffer gas mitigation, ion energy distributions have been measured for the EUV-induced background plasma by van de Ven et al.[36] Pressures in the scanner are considerably lower than in the EUV source, so these energies may be considered an upper bound to hydrogen ion energies that may be incident to the collector surface.

The maximum ion energy seen was 20 eV for the H^+ ion. This higher energy tail was attributed to the lighter mass of the H^+ ion, which allows it to react faster to the ambipolar electric field that develops in the electron wake. The heavier hydrogen ions H_2^+ and H_3^+ have a maximum energy of $\sim$10 eV. These values are too low to cause sputtering in the MLM. Hypothetically, within the EUV source there may be higher-energy hydrogen ions due to the ambipolar field generated from the LPP. With higher pressure and more collisions, hydrogen ion energies may develop akin to the previously mentioned RF plasma.

The work of Elg et al. with the RF plasma and its hundreds of eV ion energies necessitated investigation into the effect of high-energy hydrogen ion bombardment on the MLM surface.[32] Calculations of the sputtering yield for common capping materials resulted in only potential damage to Si-based capping layers. To justify this conclusion, commercially available MLMs (ZrN capped) were exposed to the RF hydrogen plasma, with secondary-ion mass spectroscopy (SIMS) performed before and after exposure. The depth profiles from the 12-keV ion beam can be used to investigate which elements are present within the sample and whether implantation, erosion, or intermixing had occurred due to RF plasma exposure. The results are shown in Fig. 18.21.

The ZrN-capped sample that was exposed to hydrogen did not show erosion of the capping layer or implantation of the hydrogen ions. Intermixing effects (which show up as smoothing of curves) are attributed to the 12-keV oxygen ion beam used to burrow into the sample during SIMS. An additional concern, hydrogen blistering of the capping layer, was investigated by using a scanning electron microscope (SEM) to evaluate the surface layer after hydrogen plasma exposure. Indeed, Fig. 18.22 shows an example of implantation and blistering in a SiN-capped sample but nothing in the ZrN-capped sample. This suggests that the SIMS data are accurate. Compatibility of the collector with hydrogen ion energies seen in the RF

Downloaded From: https://www.spiedigitallibrary.org/ebooks/ on 11 Oct 2023
Terms of Use: https://www.spiedigitallibrary.org/terms-of-use

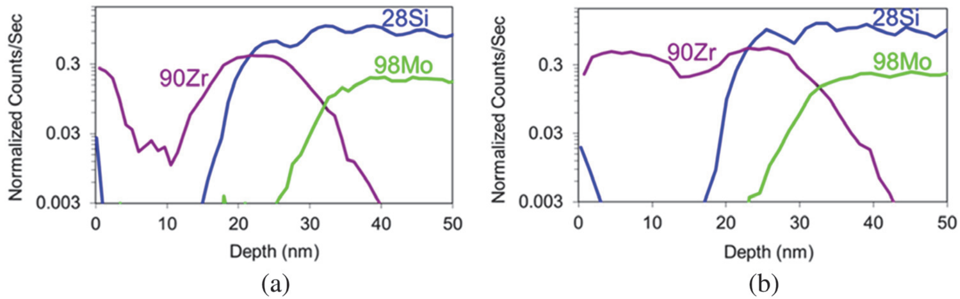

Figure 18.21 SIMS depth profiles of (a) as-received ZrN-capped MLM samples and (b) a ZrN-capped MLM sample exposed to a RF hydrogen plasma with ion energies in the hundreds of eV. There is no evidence of capping layer erosion nor of plasma-induced intermixing below the capping layer (depth of a few nanometers). Any intermixing effects in the graphs are attributed to the SIMS ion beam. (Reprinted from Ref. 32 with permission of AIP Publishing.)

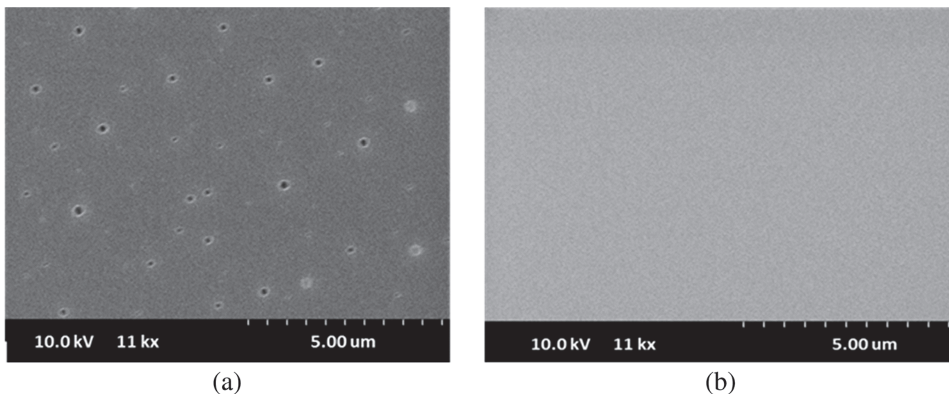

Figure 18.22 SEM images of (a) a SiN-capped MLM and (b) a ZrN-capped MLM. Both samples were exposed to a RF hydrogen plasma. Blistering can be seen in the SiN sample, while the surface of the ZrN sample is pristine. (Reprinted from Ref. 32 with permission of AIP Publishing.)

plasma cleaning technique indicates compatibility with hydrogen ions created from EUV-induced plasma and the SWP technique as both have lower energies.

18.6 Summary

Extreme-ultraviolet lithography is the next-generation technique that is carrying high-volume manufacturing to the 7-nm node and beyond. The transition to 13.5-nm photons requires a new generation of optics as well: multilayer Mo/Si mirrors that utilize Bragg reflection. The first mirror in the optical chain, the collector, is subjected to the environment of the EUV

Downloaded From: https://www.spiedigitallibrary.org/ebooks/ on 11 Oct 2023
Terms of Use: https://www.spiedigitallibrary.org/terms-of-use

source. The Sn plasma that is required for EUV photon generation also creates energetic ions and neutral fluxes that can damage the collector. Tin particles will also deposit on the collector surface, lowering reflectivity.

Debris mitigation is required to maintain tool availability at levels needed for HVM. Two forms of debris mitigation have been investigated: magnetic mitigation and buffer gas mitigation. Magnetic mitigation has shown to be effective in reducing the energy and flux of ions in the keV range but cannot deflect the neutral tin that incorporates ~99% of total debris in the source. Buffer gas was chosen as it has been shown to reduce flux and energy of neutral and charged debris in the EUV source. Industrial buffer gas mitigation has successfully extended the collector lifetime.

Unfortunately, buffer gas cannot prevent all deposition on the collector surface from the EUV plasma. Agglomeration of tin into larger particles and ejection from other surfaces can occur and cannot be stopped by the hydrogen flow. These particles accumulate on the collector surface and degrade reflectivity of the optic. Currently, *ex situ* cleaning of the collector is the preferred reflectivity-restoration method by industry. To decrease downtime, *in situ* methods using hydrogen radicals have been proposed and researched in the past. Hydrogen radicals react with tin to form a gaseous SnH_4 that can be pumped out of the vessel. While this method can be used to reverse the reflectivity degradation, a large number of external radicals would need to be introduced to the EUV source to etch the tin debris occurring in HVM. At the moment, no technique has been able to produce these etch rates with externally supplied radicals alone.

Hydrogen-plasma-based techniques have been proposed to enhance the etch rate in the EUV source, creating chemically reactive species at the surface to be cleaned. The first plasma-based method covered in this chapter uses the collector itself as a RF plasma electrode. The plasma is able to etch the tin film and restore reflectivity of the MLM samples. Additionally, the etch rate is found to scale with hydrogen ion energy flux, not hydrogen radical flux. A surface-wave plasma is then proposed to maximize ion energy flux to the collector surface. While the etch rate is enhanced, the low-powered plasma is only able to cover maybe 10% of the collector. Work is ongoing to cover the entire collector with hydrogen plasma for etching purposes, using more power and new SWP antenna designs.

Finally, the damage mechanisms due to the ion flux from hydrogen-plasma-based cleaning or EUV-induced background plasma were investigated. SIMS depth profiles of ZrN-capped MLM samples show zero erosion or implantation from incident hydrogen plasma ions with an average energy of 250 eV. SEM images show implantation and blistering on SiN-capped MLM samples but show a pristine surface on the ZrN-capped samples. ZrN-capped multilayer mirrors have thus shown compatibility with hydrogen plasma in that they can resist damage from hydrogen ions.

Downloaded From: https://www.spiedigitallibrary.org/ebooks/ on 11 Oct 2023
Terms of Use: https://www.spiedigitallibrary.org/terms-of-use

Much development is still needed before EUV can replace DUV in all steps required at the smallest pitches for HVM, but the achievements to date have been remarkable. The collector lifetime for ASML's NXE:3300 EUV source was initially only a minute (3 megapulses). Now the collector lifetime in ASML sources can be measured in months. Future work toward optimization of buffer gas implementation and additional cleaning techniques should continue to further increase collector lifetime. Once the collector lifetime outpaces other tool availability concerns, EUV can take the final step toward HVM integration.

References

1. "Encyclopedia Britannica," [online] https://www.britannica.com/technology/computer/Transistor-size.
2. A. Pirati, R. Peeters, D. Smith, et al., "EUV lithography performance for manufacturing: status and outlook," *Proc. SPIE* **9776**, 97760A (2016) [doi: 10.1117/12.2220423].
3. D. T. Attwood, *Soft X-rays and Extreme Ultraviolet Radiation: Principles and Applications*, Cambridge University Press (2009).
4. K. Yamamoto, "Optical visualization of acoustic fields: the schlieren technique, the Fresnel method and the photoelastic method applied to ultrasonic transducers," in *Ultrasonic Transducers*, K. Nakamura, Ed., Woodhead Publishing, pp. 314–328 (2012).
5. E. Louis, A. E. Yashkin, P. C. Goerts, et al., "Progress in Mo/Si multilayer coating technology for EUVL optics," *Proc. SPIE* **3997**, pp. 406–411 (2000) [doi: 10.1117/12.390077].
6. J. A. Folta, S. Bajt, T. W. Barbee, Jr., et al., "Advances in multilayer reflective coatings for extreme-ultraviolet lithography," *Proc. SPIE* **3676**, pp. 702–709 (1999) [doi: 10.1117/12.3511565].
7. B. L. Henke, "Multilayer Reflectivity," Center for X-Ray Optics, [Online] https://henke.lbl.gov/optical_constants/multi2.html.
8. K. Motai, H. Oizumi, S. Miyagaki, et al., "Atomic hydrogen cleaning of Ru-capped EUV multilayer mirror," *Proc. SPIE* **6517**, 65170F (2007) [doi: 10.1117/12.711998].
9. M. A. van de Kerkhof, F. Liu, M. Meeuwissen, et al., "High-power EUV lithography: spectral purity and imaging performance," *J. Micro/Nanolith., MEMS, MOEMS* **19**(3), 033801 (2020) [doi: 10.1117/1.JMM.19.3.033801].
10. S. Yulin, N. Benoit, T. Feigl, and N. Kaiser, "Interface-engineered EUV multilayer mirrors," *Microelectronic Engineering* **83**(4–9), 692–694 (2006).
11. B. Kneer, S. Migura, W. Kaiser, J. T. Neumann, J. van Schoot, et al., "EUV lithography optics for sub-9nm resolution," *Proc. SPIE* **9422**, 94221G (2015) [doi: 10.1117/12.2175488].

Downloaded From: https://www.spiedigitallibrary.org/ebooks/ on 11 Oct 2023
Terms of Use: https://www.spiedigitallibrary.org/terms-of-use

12. S. N. Srivastava, K. C. Thompson, E. L. Antonsen, H. Qui, J. B. Spencer, D. Papke, and D. N. Rusic, "Lifetime measurements on collector optics from Xe and Sn extreme ultraviolet sources," *J. Appl. Phys*. **102**(2), 023301 (2007).
13. R. A. Burdt, Y. Tao, M. S. Tillack, et al., "Laser wavelength effects on the charge state resolved ion energy distributions form laser-produced Sn plasma," *J. Appl. Phys*. **107**(4), 043303 (2010).
14. D. N. Ruzic, K. C. Thompson, B. E. Jurczyk, et al., "Reduction of ion energies from a multicomponent *Z*-pinch plasma," *IEEE Transactions on Plasma Science* **35**(3), 606–613 (2007).
15. A. Roy, S. M. Hassan, S. S. Harilal, et al., "Extreme ultraviolet emission and confinement of tin plasmas in the presence of a magnetic field," *Physics of Plasmas* **21**(5), 053106 (2014).
16. A. Endo, H. Hoshino, T. Suganuma, et al., "Laser-produced EUV light source development for HVM," *Proc. SPIE* **6517**, 65170O (2007) [doi: 10.1117/12.711097].
17. Y. Nishimura, T. Hori, T. Yabu, et al., "Key components development progress of high-power LPP-EUV light source with unique debris mitigation system using a magnetic field," *Proc. SPIE* **10809**, 108091M (2018) [doi: 10.1117/12.2500356].
18. J. R. Sporre, "Diagnosis of the flux emanating from the intermediate focus of an extreme ultraviolet light lithography source," Ph.D. thesis, University of Illinois Urbana-Champaign (2013).
19. J. R. Sporre, D. T. Elg, K. K. Kalathiparambil, and D. N. Ruzic, "Modeling and measuring the transport and scattering of energetic debris in an extreme ultraviolet plasma source," *J. Micro/Nanolith. MEMS MOEMS* **15**(1), 013503 (2016) [doi: 10.1117/1.JMM.15.1.013503].
20. I. Fomenkov, "EUV source for lithography: readiness for HVM and outlook for increase in power and availability," presented at the 2018 EUV Source Workshop, Prague, https://www.euvlitho.com/2018/S1.pdf.
21. D. C. Brandt, M. Purvis, I. Fomenkov, et al., "Advances toward high power EUV sources for EUVL scanners for HVM in the next decade and beyond," *Proc. SPIE* **11609**, 116091E (2021) [doi: 10.1117/12.2584413].
22. J. W. Gallagher, C. E. Brion, J. A. R. Samson, and P. W. Langhoff, "Absolute cross sections for molecular photoabsorption, partial photoionization, and ionic photofragmentation processes," *J. Physical and Chemical Reference Data*. **17**(1), 9 (1988).
23. M. M. J. W. van Herpen, D. J. W. Klunder, W. A. Soer, R. Moors, and V. Banine, "Sn etching with hydrogen radicals to clean EUV optics," *Chemical Physics Letters* **484**(4–6), 197–199 (2010).
24. K. Tamaru, "The thermal decomposition of tin hydride," *J. Physical Chemistry* **60**(5), 610–612 (1956).

Downloaded From: https://www.spiedigitallibrary.org/ebooks/ on 11 Oct 2023
Terms of Use: https://www.spiedigitallibrary.org/terms-of-use

25. J. W. Coburn and H. F. Winters, "Ion and electron assisted gas surface chemistry: an important effect in plasma etching," *J. Appl. Phys.* **50**(5), p. 3189 (1979).
26. H. Shin, S. N. Srivstava, and D. N. Ruzic, "Tin removal from extreme ultraviolet collector optics by inductively coupled plasma reactive ion etching," *J. Vac. Sci. Tech. A* **26**(3), 389 (2008).
27. K. J. Laidler, "Mechanisms of surface-catalyzed reactions," *J. Physical Chemistry* **57**(3), 320–321 (1953).
28. J. R. Sporre, D. Elg, D. Andruczyk, T. Cho, D. N. Ruzic, S. Srivastava, and D. C. Brandt, "In-situ Sn contamination removal by hydrogen plasma," *Proc. SPIE* **8322**, 83222L (2012) [doi: 10.1117/12.916434].
29. D. T. Elg, F. A. Panici, S. Liu, G. Girolami, S. N. Srivastava, and D. N. Ruzic, "Removal of tin from extreme ultraviolet collector optics by in-situ hydrogen plasma etching," *Plasma Chemistry and Plasma Processing* **38**(1), 223–245 (2018).
30. D. T. Elg, G. A. Panici, J. A. Peck, S. N. Srivastava, and D. N. Ruzic, "Modeling and measurement of hydrogen radical densities of *in situ* plasma-based Sn cleaning source," *J. Micro/Nanolith., MEMS, MOEMS* **16**(2), 023501 (2017) [doi: 10.1117/1.JMM.16.2.023501].
31. D. Ugur, A. J. Storm, R. Verberk, J. C. Brouwer, and W. G. Sloofe, "Generation and decomposition of volatile tin hydrides monitored by *in situ* quartz crystal microbalances," *Chemical Physics Letters* **552**, 122–125 (2012).
32. D. T. Elg, J. R. Sporre, G. A. Panici, S. N. Srivastava, and D. N. Ruzic, "*In situ* collector cleaning and extreme ultraviolet reflectivity restoration by hydrogen plasma for extreme ultraviolet sources," *J. Vac. Sci. Tech. A* **34**(2), 021305 (2016).
33. G. Panici, D. Qerimi, and D. N. Ruzic, "Ongoing investigation of collector cleaning by surface wave plasma in the Illinois NXE:3100 chamber," *Proc. SPIE* **10957**, 109571B (2019) [doi: 10.1117.12.2515072].
34. G. Panici, D. Qerimi, and D. N. Ruzic, "Study of Sn removal by surface wave plasma for source cleaning," *Proc. SPIE* **10143**, 10143121 (2017) [doi: 10.1117/12.2258065].
35. G. Panici, D. Qerimi, and D. N. Ruzic, "Study of Sn removal by surface wave plasma for source cleaning (Conference Presentation)," *Proc. SPIE* **10583**, 10583 (2018) [doi: 10.1117/12.2297458].
36. T. H. M. van de Ven, P. Reefman, C. A. de Meijere, et al., "Ion energy distributions in highly transient EUV induced plasma in hydrogen," *J. Appl. Phys.* **23**(6) (2018).

Downloaded From: https://www.spiedigitallibrary.org/ebooks/ on 11 Oct 2023
Terms of Use: https://www.spiedigitallibrary.org/terms-of-use

David N. Ruzic is the Abel Bliss Professor of Engineering and has been in the Department of Nuclear, Plasma, and Radiological Engineering at the University of Illinois Urbana-Champaign (UIUC) since 1984 after receiving his Ph.D. in Physics from Princeton University and performing post-doctoral work at the Princeton Plasma Physics Laboratory. His research centers on the interaction of plasmas with materials. He is a Fellow of the American Nuclear Society, the American Vacuum Society, the American Physical Society, and SPIE. In 2020 he won the international Gaede-Langmuir award from the AVS and the Fusion Technology Prize from IEEE. He has published over 220 referred journal papers, 2 books, and 6 book chapters, and has been awarded 11 patents. He has produced 36 Ph.D. students and 59 thesis M.S. students. His current group consists of 1 research scientist, and 15 graduate and 25 undergraduate research assistants. In 2017, he headed the effort to bring a mid-sized hybrid stellarator/tokamak to Illinois, now called HIDRA, capable of 1-Tesla fields with a minor radius of 19 cm and a major radius of 72 cm. In 2020, he founded the Illinois Plasma Institute located on the UIUC Research Park, which is funded by industry to do translational research.

Gianluca Panici received his Ph.D. from the Department of Nuclear, Plasma, and Radiological Engineering at the University of Illinois Urbana-Champaign. His dissertation topic was on the influence of hydrogen ions on tin etching with a focus on collector cleaning using an *in situ* surface-wave plasma source. He also received his M.S. and B.S. degrees from the Nuclear, Plasma, and Radiological Engineering department at the University of Illinois. Gianluca currently works for Lam Research.

Downloaded From: https://www.spiedigitallibrary.org/ebooks/ on 11 Oct 2023
Terms of Use: https://www.spiedigitallibrary.org/terms-of-use